1
2

A modified strain-softening model with multi-post-peak behaviors and its application in circular tunnel

5
6

Xuezhen Wu[1, 2], Yujing Jiang[2, 3] [*], Zhenchang Guan[1]

8

[1] *College of Civil Engineering, Fuzhou University, Fuzhou 350108, China*

[2] *Graduate School of Engineering, Nagasaki University, Nagasaki 852-8521, Japan;*

[3] *State Key Laboratory of Mining Disaster Prevention and Control Co-founded by Shandong Province and the Ministry of Science and Technology, Shandong University of Science and Technology, Qingdao 266590, China;*

13

Corresponding author: Yujing Jiang

Corresponding Address: Bunkyo Machi 1-14, Nagasaki 852-8521, Japan.

Email: jiang@nagasaki-u.ac.jp

Phone: +81-080-3118-5202

Fax: +0532-86057957

19

First author: Xuezhen Wu, Email: wu@fzu.edu.cn

Third author: Zhenchang Guan, Email: zcguan@fzu.edu.cn

22

23

A modified strain-softening model with multi-post-peak behaviors and its application in circular tunnel

Abstract: A large number of laboratory experiments have shown that the rocks in post-peak state present strain-softening behaviour under low confining pressure, and gradually evolved into elastic-perfectly plastic with the increasing of confining pressure. Neither the elastic-perfectly plastic model nor the strain-softening model can accurately describe the behavior of rock mass surrounding the deep buried excavations. In this paper, a modified strain-softening model was proposed to describe the non-linear evolution of residual strength under the influence of confining pressure. The new model can realize the gradually transition from strain-softening behaviour to elastic-perfectly plastic behaviour with the increasing of confining pressure. The equivalent residual strength was defined to quantify the strength of rocks in post-peak stage. The parameters involved in the model were estimated via non-linear regression analysis upon a series of stress-strain curves. Based on the plane strain axial symmetry assumption and the incremental theory of plasticity, equilibrium equations and compatibility equations of rock mass around a circular tunnel were deduced. The equations were implemented in the Visual Basic development environment, and a semi-analytical solution was obtained. The influence of post-failure behavior of rock mass was demonstrated through an illustrative case. The distributions of stress, displacement and transitional strength around the tunnel were presented. The differences between the elastic-perfectly plastic model, the strain-softening model and the new model were estimated quantitatively. In addition, the validity of semi-analytical solution was verified by numerical simulations. Parameters analysis showed that the tunnel convergence was influenced by the post-peak behaviour of rock mass dramatically.

Keywords: strain-softening model; post-peak behavior; confining pressure; residual strength; semi-analytical solution

1 Introduction

The post-peak behavior is important in engineering practice as the rocks surrounding deep buried excavations (particularly within the excavation damaged zone, EDZ) are basically in

51 post-peak state (Hao et al., 2016; Wu et al. 2018). For an effective engineering design, it is

52 necessary to take into account the real mechanical behavior of rocks in post-failure states (Troncone

53 et al., 2014).

54   A large number of laboratory experiments have been conducted to explore the post-failure

55 behavior of rocks (Fang and Harrison, 2001; Yang et al., 2008; Li et al., 2011; Walton et al., 2015;

56 Cheng et al., 2016; Zimbardo, 2016; Peng et al., 2017). The stress-strain curves obtained in

57 compression tests descended towards a residual state with the increasing of axial strain after

58 attainment of the peak stress (Tiwari et al., 2006; Alejano et al., 2010; Li et al., 2011; Tutluoğlu et

59 al., 2015). The peak strength increased almost linearly with the increasing of confining pressure in

60 most of the laboratory tests. Generally, confining pressure means minimum principal stress σ_3

61 (Zhang et al., 2018). However, the evolution of residual strength was quite different, which

62 increased more quickly with the increasing of confining pressure (Tiwari et al., 2006; Ma et al.,

63 2014). The rocks present strain-softening features under low confining pressure, while gradually

64 evolved into elastic-perfectly plastic with the increasing of confining pressure (Kaiser et al., 2015).

65   The transition from brittle to ductile behavior of rocks is a fundamental feature of rock

66 mechanics. An accurate prediction of rock strength is essential for the understanding of many

67 processes encountered in geological sciences and rock engineering (Wang et al., 2002; Wu et al.

68 2017). However, only elastic-perfectly plastic model or strain-softening model were available to

69 describe the rock behaviors in the past studies (Alonso et al., 2003; Varas et al., 2005). When a

70 tunnel was excavated, the excavation effect could lead to a complex non-uniform stress field around

71 the excavation. Neither the elastic-perfectly plastic model nor the strain-softening model can

72 accurately describe the behavior of rocks surrounding the deep buried excavation. Moreover, few

73 research was found to describe the influence of the multi-post-peak behaviors of rock mass in the

74 ground reaction analyse (Cui et al., 2017).

75   In order to express the non-linear behaviour of rocks, the mechanical behaviour of the basic

76 elements should be variable under different loading conditions (Saksala et al., 2014; Li et al., 2012).

77 Fang and Harrison (2001) defined a strength degradation index to describe the variation of strength

78 degradation behaviour with different confining pressures. The strength degradation index was

79 expressed as the ratio between the actual strength degradation and maximum strength degradation.

80 However, it is difficult to use the strength degradation index in engineering calculations. The

81 influence of post-failure behavior of rock mass is still unclear in actual engineering practice.

82 Alejano et al. (2009) introduced three strain softening models including constant strength drop

83 modulus and constant dilatancy, variable drop modulus and constant dilatancy, variable drop

84 modulus and variable dilatancy. The third one was considered to represent a more general behaviour

85 of rock mass. However, the relationship of residual strength and confining pressure is still linearly

86 dependent, which is not coincidence with the actual rock behaviour.

87   The constitutive equations for rocks in previous studies are unable to express the non-linear

88 evolution of residual strength. Juang et al. (2013) proposed a Bayesian framework using field

89 observations by updating of soil parameters, which gave a revelation to the study of

90 post-failure behavior of rocks. In this paper, a modified strain-softening model was proposed to

91 describe the strength evolution from pre-failure to residual stages considering the influence of

92 confining pressure. The key feature of this model is the gradual transition from strain-softening

93 features to elastic-perfectly plastic with the increasing of confining pressure. The influence of

94 multi-post-failure behaviors was demonstrated in ground reaction analyses.

95 **2 A modified strain-softening model**

96   The conventional strain-softening behavior was often simplified to the form of three line

97 segments as shown in Fig. 1. Generally, the rocks exhibiting strain-softening behavior was

98 characterized by a yielding criterion $f(\sigma_{ij}, \alpha)$ and a plastic potential $g(\sigma_{ij}, \alpha)$. α is a softening

99 parameter controlling the gradual transition of rock from a peak failure criterion to a residual one.

100 Herein, the rock is assumed to satisfy the linear Mohr-Coulomb criterion and linear plastic potential.

101 The major principal plastic strain ε_l^p is employed as the softening parameter. It can be obtained

102 easily from the results of triaxial compression tests. Therefore, the failure criterion f and the plastic

103 potential g can be formulated as follows (Alonso1 et al., 2003; Guan et al., 2007a).

104
$$f = \sigma_1 - K_p\sigma_3 - \sigma_c = \begin{cases} \sigma_1 - K_p\sigma_3 - \left(\sigma_c^1 + \dfrac{(\sigma_c^1 - \sigma_c^2)\varepsilon_1^{\,p}}{\alpha\varepsilon_{1e}} \right) & (0 \le \varepsilon_1^{\,p} \le \alpha\varepsilon_{1e}) \\ \sigma_1 - K_p\sigma_3 - \sigma_c^2 & (\varepsilon_1^{\,p} \ge \alpha\varepsilon_{1e}) \end{cases}$$
(1)

105
$$g = \sigma_1 - K_\psi\sigma_3 = \begin{cases} \sigma_1 - K_\psi^1\sigma_3 & (0 \le \varepsilon_1^{\,p} \le \alpha\varepsilon_{1e}) \\ \sigma_1 - K_\psi^2\sigma_3 & (\varepsilon_1^{\,p} \ge \alpha\varepsilon_{1e}) \end{cases}$$
(2)

106   In the above equations, K_p is the passive coefficient and remains unchanged within the

107 complete plastic region. K_p equals to $(1 + \sin\varphi)/(1 - \sin\varphi)$, where φ is friction angle of rock. σ_c is

108 the compression strength, which changes gradually from σ_c^1 to σ_c^2, according to the evolution of the

109 major principal plastic strain ε_l^p. K_ψ is the dilation factor, and equals to K_ψ^1 and K_ψ^2 for softening

110 region and residual region, respectively.

111
112   (a)   (b)
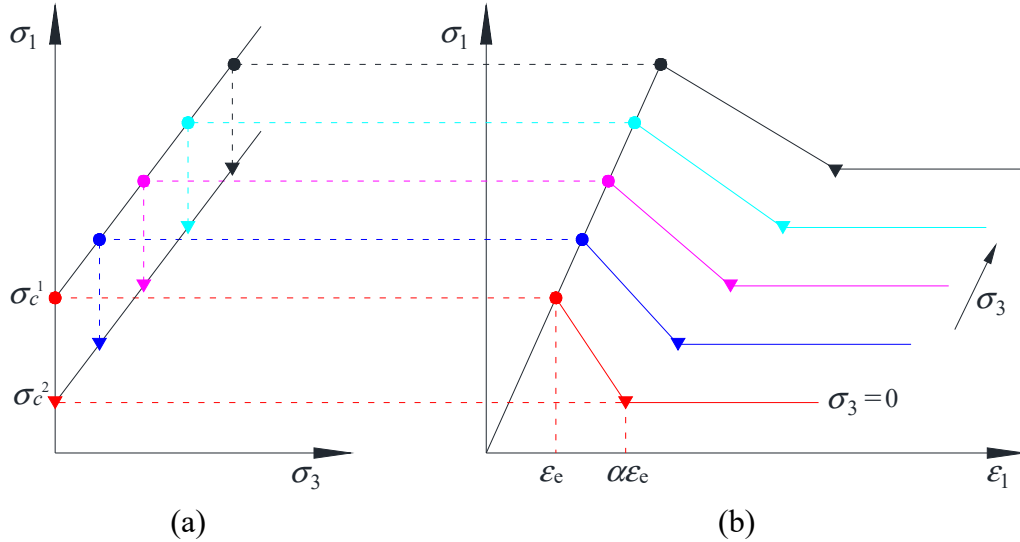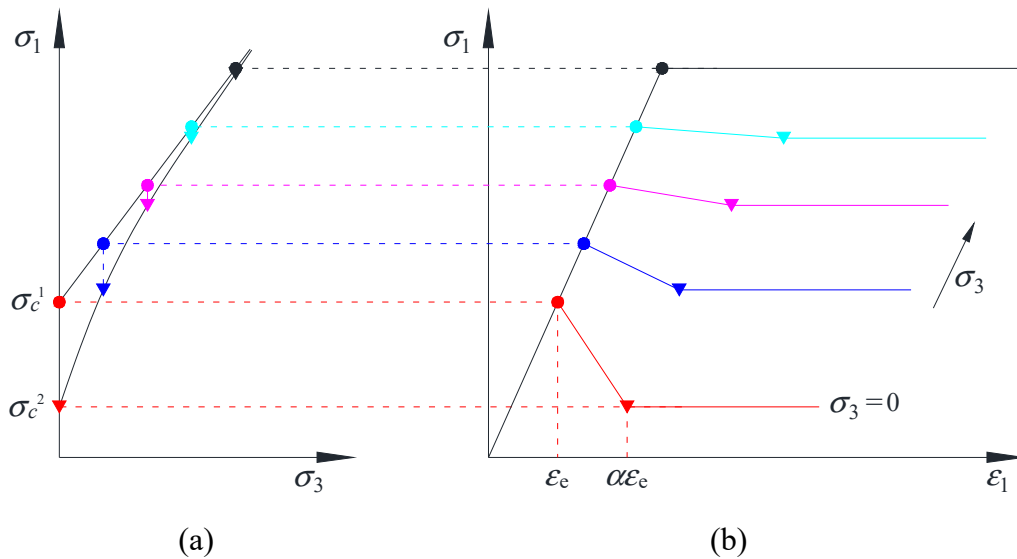
113   Fig. 1 Conventional strain-softening model: (a) evolution of strength with confining pressure;

114   (b) constitutive relation

115

116   (a)   (b)
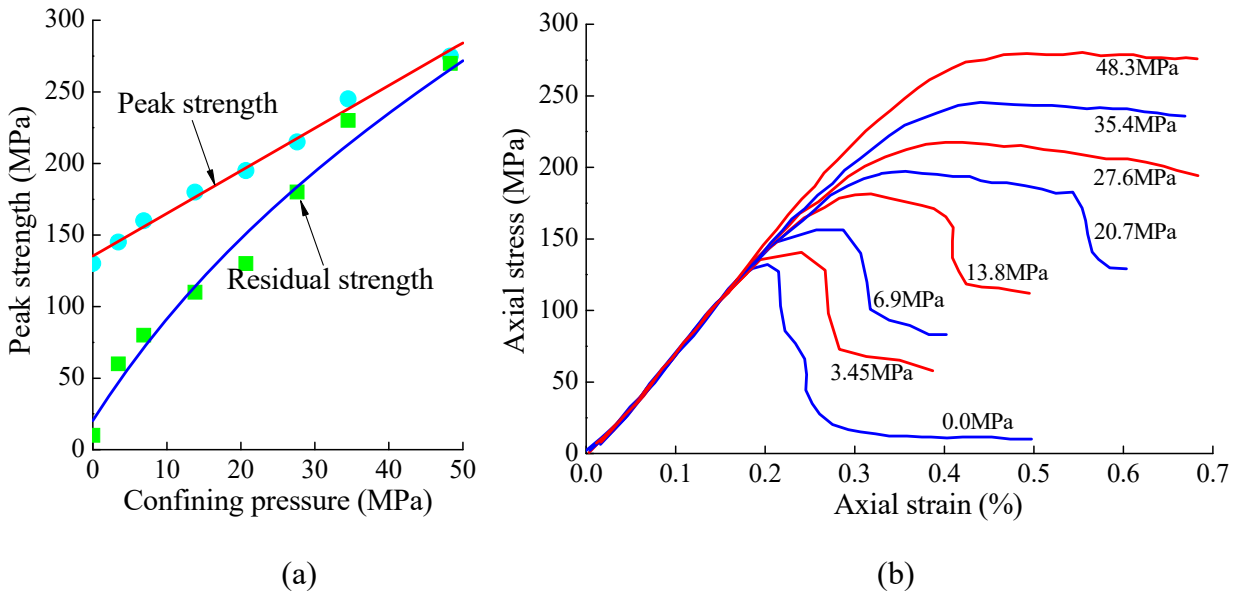
117   Fig. 2 Tennessee marble under common triaxial compression: (a) evolution of rock strength

118   with confining pressure; (b) complete axial stress-strain curves (Fang and Harrison, 2001).

119   With the increasing of confining pressure, both the peak strength and residual strength

120 increased linearly in conventional strain-softening model as shown in Fig. 1a. However, the actual

121 behavior is quite different in high confining pressure environment where the rock becomes fully

122 ductile, and showing almost no strength reduction after failure as shown in Fig. 2 (Fang and

Harrison, 2001; You et al., 2007). Fig. 2b showed a set of stress-strain curves for Tennessee marble obtained in triaxial compression tests with different confining pressures (Fang and Harrison, 2001). The peak strength increased almost linearly with the increasing confining pressure as shown in Fig. 2a. In contrast, the residual strength increased from considerably low values, and approached the peak strength in a non-linear manner. Finally, the rock became fully ductile at high confining pressure, showing almost no strength reduction after failure. Similar behavior was observed in many other test results (You, 2007). These laboratory tests have shown that the residual strength is more sensitive to the increasing of confining pressure than the peak strength. It is necessary to establish a non-linear relationship between the confining pressure and the residual strength.

(a)   (b)

Fig. 3 A modified strain-softening model: (a) evolution of strength with confining pressure; (b) constitutive relation.

(a)   (b)
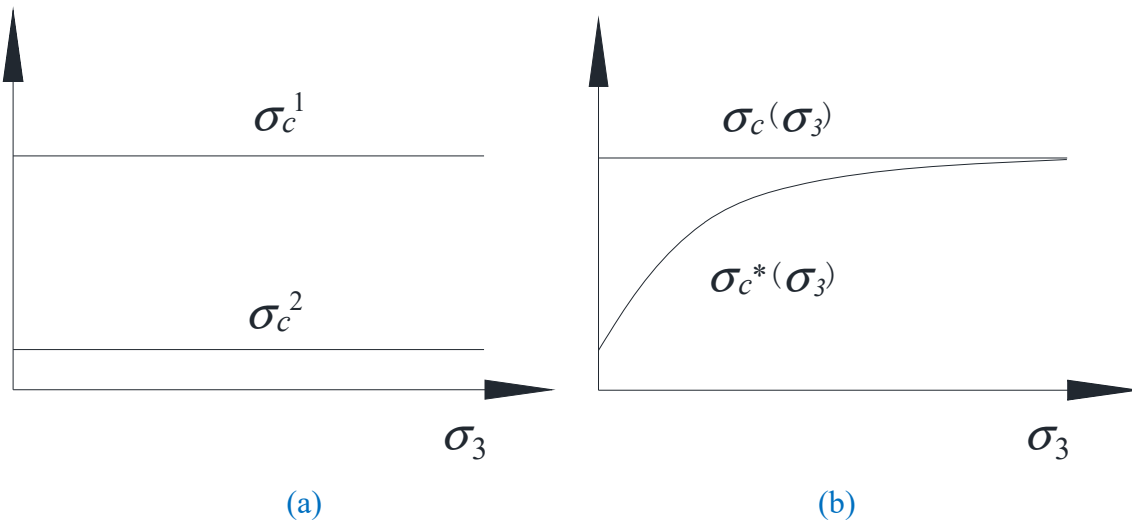
Fig. 4 The equivalent residual strength of rock: (a) conventional strain-softening model;

139   (b) modified strain-softening model.

140   A modified strain-softening model was proposed to describe the evolution of residual strength

141 with the increasing of confining pressure as shown in Fig. 3. In the new model, the strain-softening

142 behavior was also approximated as three line segments, but the evolution of residual strength was

143 governed by a non-linear equation. In the stage before peak strength, the equation was the same as

144 the conventional strain-softening model.

145   A new variable was defined as equivalent peak strength $\sigma_c(\sigma_3)$ to get rid of the linear influence

146 of confining pressure as shown in equation (3). Similarly, equivalent residual strength $\sigma_c^*(\sigma_3)$ was

147 defined as shown in equation (4). Fig. 4a shows that both the equivalent peak strength and the

148 equivalent residual strength are constants in the conventional model. In the new model, the

149 equivalent peak strength $\sigma_c(\sigma_3)$ is a constant, while the equivalent residual strength $\sigma_c^*(\sigma_3)$ is a

150 function of confining pressure in the post-failure process as shown in Fig. 4b.

151 $$\sigma_c(\sigma_3) = \sigma_c - K_p * \sigma_3 \qquad (3)$$

152 $$\sigma_c^*(\sigma_3) = \sigma_c^* - K_p * \sigma_3 \qquad (4)$$

153 Where, σ_c is the peak compression strength, and σ_c^* is residual compression strength in laboratory

154 tests. K_p is the confinement coefficient, which remains unchanged within the plastic region. K_p and

155 $\sigma_c(\sigma_3)$ can be obtained by linear regression based on the relation of σ_1 and σ_3 as shown in equation

156 (5).

157 $$\sigma_1 = K_p * \sigma_3 + \sigma_c(\sigma_3) \qquad (5)$$

158   Considering the influence of confining pressure on residual strength, the constitutive relations

159 for the modified strain-softening model can be given as follows:

160 $$\sigma_1 = \begin{cases} K_p\sigma_3 + \left(\sigma_c(\sigma_3) + \dfrac{(\sigma_c(\sigma_3) - \sigma_c^*(\sigma_3))\varepsilon_1^p}{\alpha\varepsilon_{1e}} \right) & (0 \leq \varepsilon_1^p \leq \alpha\varepsilon_{1e}) \\ K_p\sigma_3 + \sigma_c^*(\sigma_3) & (\varepsilon_1^p \geq \alpha\varepsilon_{1e}) \end{cases} \qquad (6)$$

161   In the above equations, the compression strength transits gradually from $\sigma_c(\sigma_3)$ to $\sigma_c^*(\sigma_3)$,

162 according to the evolution of the major principal plastic strain ε_l^p. Herein, the major principal

163 plastic strain ε_l^p is employed as the softening parameter, as it can be obtained easily from the results

164 of triaxial compression tests. K_p is the passive coefficient.
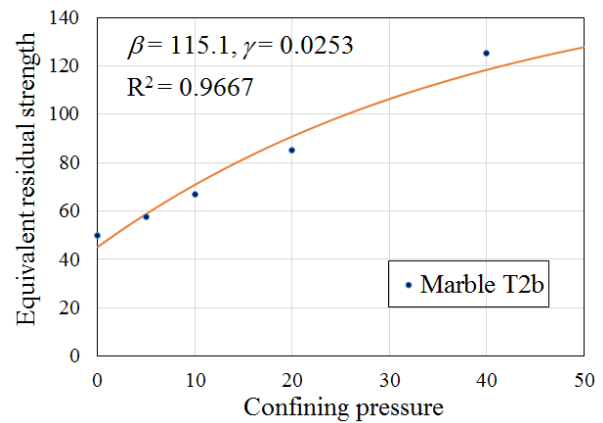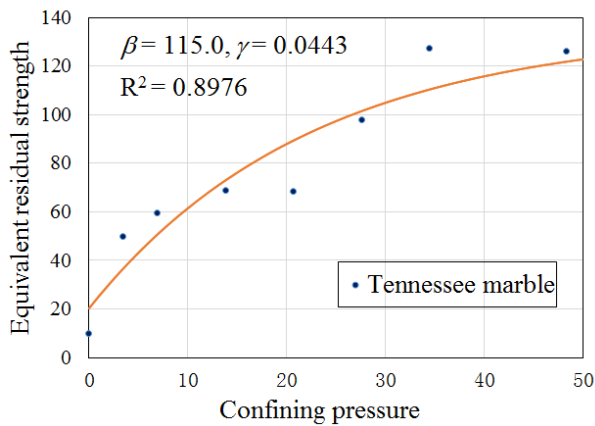
165   The equivalent residual strength $\sigma_c^*(\sigma_3)$ could be estimated based on the laboratory test data in

166   existing literatures. Based on laboratory experimental data, it is suggested that the relation between

167   the equivalent residual strength and confining pressure could be expressed by equation (7).

168

$$\sigma_c^*(\sigma_3) = \sigma_c(\sigma_3) - \beta * e^{-\gamma*\sigma_3} \tag{7}$$

169   Where, $\sigma_c^*(\sigma_3)$ is the equivalent residual strength, σ_3 is the confining pressure, and $\sigma_c(\sigma_3)$ is

170   equivalent peak strength. The equivalent residual strength $\sigma_c^*(\sigma_3)$ for different types of rocks can

171   be calculated by equation (4), and $\sigma_c(\sigma_3)$ can be obtained according to equation (5). According to

172   the definition, the values of $\sigma_c^*(\sigma_3)$ must be less than $\sigma_c(\sigma_3)$ and gradually approaching to it.

173   β represents the difference between equivalent peak strength and equivalent residual strength when

174   the confining pressure is zero. γ is an exponential parameter, which control the transformation speed

175   of residual strength to peak strength. β and γ could be estimated by curvilinear regression based on

176   a series of stress-strain curves from triaxial compression tests.

177   For example, the source data for Tennessee marble were obtained by estimating the peak and

178   residual strengths of each stress–strain curve in Fig. 2. According to Eq. (4) and Eq. (5), the

179   equivalent peak strength and equivalent residual strength for Tennessee marble were computed and

180   tabulated in Table 1. The data for other kind of marbles, mudstone, limestone, coal and sandstone

181   were presented in Appendix A. The mathematical relationship of equivalent residual strength and

182   confining pressure was fitted to negative exponential function. The data together with the best-fit

183   curves are shown in Fig. 5. In the case of Tennessee marble, the value of β was evaluated as 115.0,

184   and the value of γ was evaluated as 0.0443 by curvilinear regression on the data listed in Table 1.

185   The correlation coefficient for this analyses is 0.8976.

186

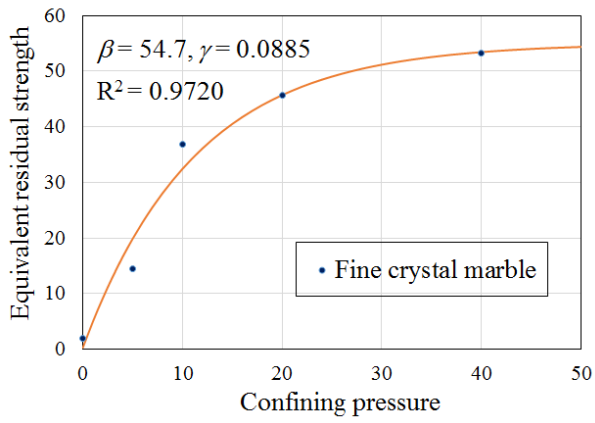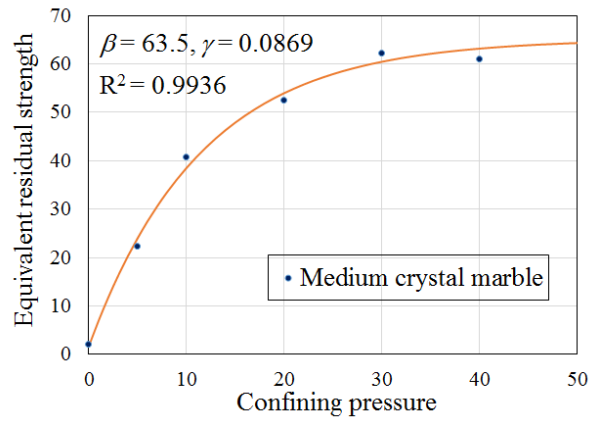187   (a)   (b)

188

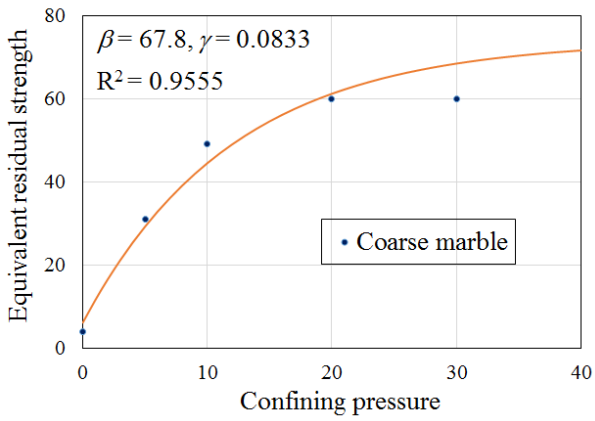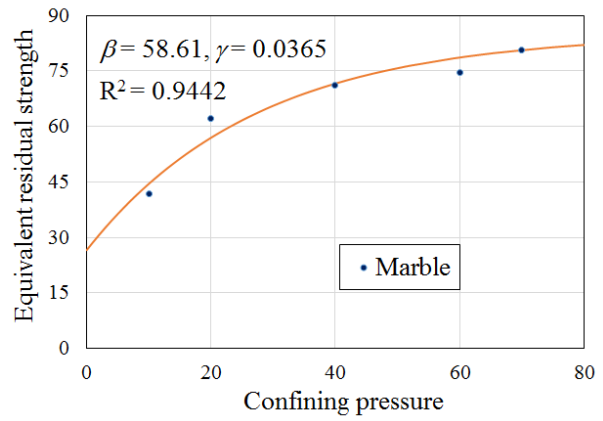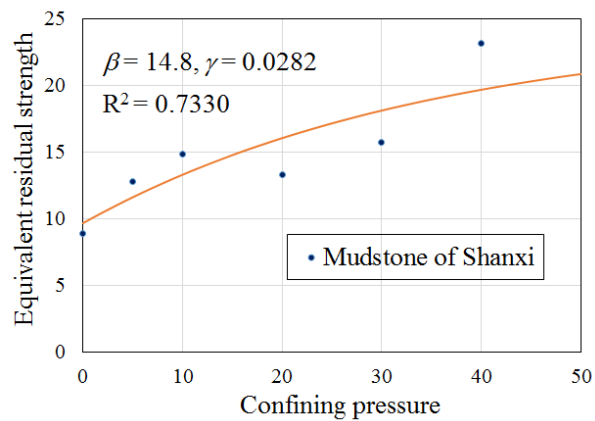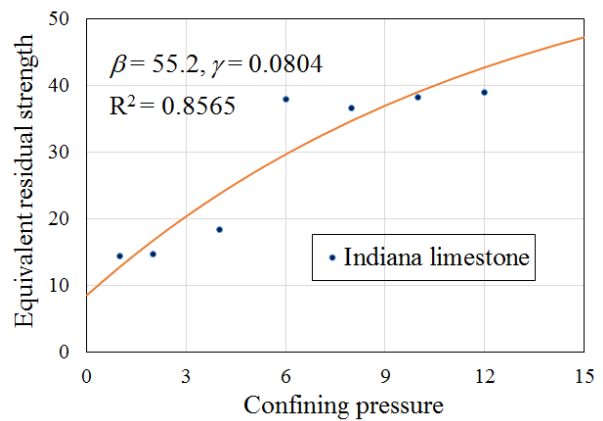189   (c)   (d)
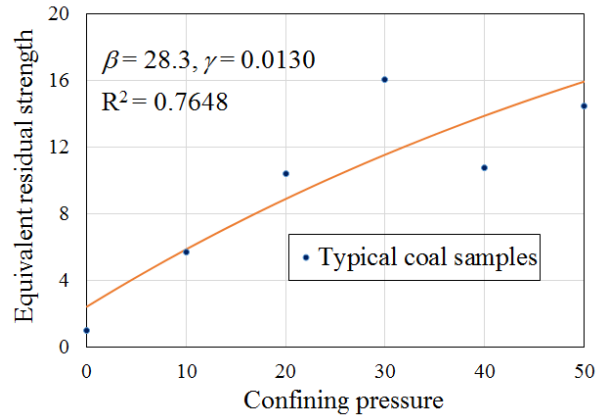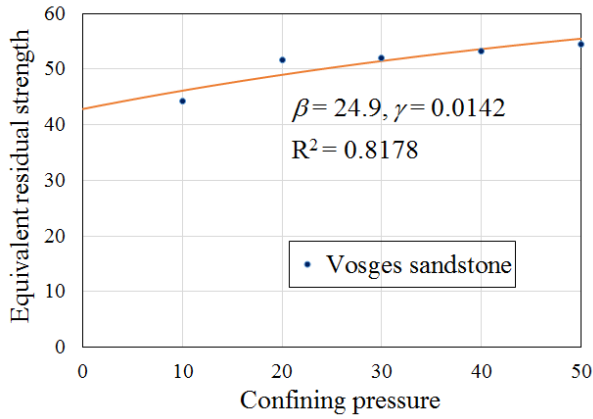

190

191   (e)   (f)

192   (Continue on next page)

193

194

195   (g)   (h)

196

197   (i)   (j)

198   Fig.5 Variation of equivalent residual strength with confining pressure for different rocks.

199   Laboratory testing was required to determine the parameters for a specific rock. The value of

200   β, γ and correlation coefficients for different types of rock were listed in Table 2. According to the

201   mathematical sense of equation (7), β represents the difference between equivalent peak strength

202   and equivalent residual strength when the confining pressure is equal to zero. However, the internal

203   instability of residual strength in uniaxial condition resulted that the equivalent residual strength is

204   quite inaccuracy. Therefore, the value of β was suggested to be determined by curvilinear

205   regression. The difference between equivalent peak strength and equivalent residual strength is just

206   a reference of β. These results implied that the value of γ range from 0.01 to 0.1. The value of

207   correlation coefficients were larger than 0.7 for all the samples, which indicated that the correlation

208   between equivalent residual strength and confining pressure was very significant. In addition, the

209   correlation coefficients were relatively higher in the case of marble than the case of mudstone,

210   limestone, sandstone and coal. The results indicated that the relation is more remarkable for hard

211   rock than soft rock. The instability behaviour of soft rock could also be confirmed by the laboratory

212   results by Indraratna (2014). Numerical simulation were conducted to reproduce the post-failure

213   behavior of the tested rock, and a better agreement was observed for the new model, especially

214   under high confining pressure conditions. Therefore, the superiority of new model was verified as

215   shown in Appendix B.

216   **3 Ground Reaction Analyses of a Circular Tunnel with the New Model**

217   **3.1 Problem Description**

218   The proposed model was applied in the ground reaction analyses of a circular tunnel to reveal

219   the influence of post-failure behavior of rock mass on the tunnel convergence. The calculation was

220   developed from the solution for circular tunnels excavated in conventional strain-softening

221   materials by the authors (Guan et al., 2007b). The excavation of long deep tunnels with circular

222   cross section under hydrostatic in-situ stress condition could be considered as an axial symmetry

223   plane strain problem.

224   **3.2 Equilibrium Equations for Rock Mass**

225   Consider an infinitesimal volume in the radial direction as shown in Fig. 6, the static

226   equilibrium condition of the infinitesimal rock mass volume can be formulated as following (Guan

227   et al., 2007b).
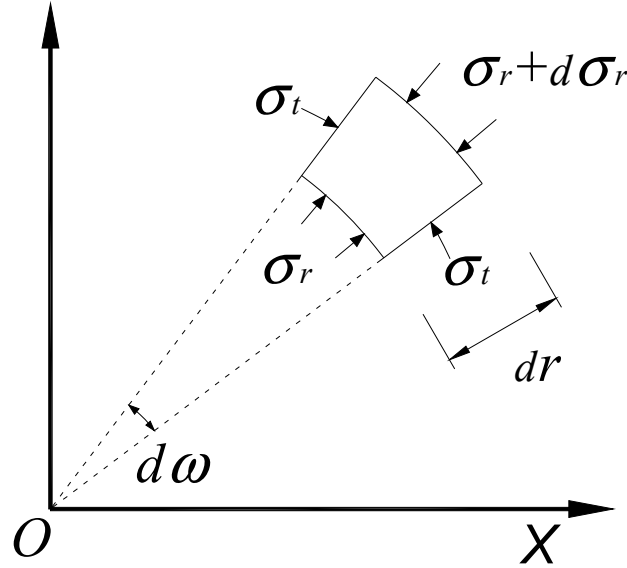
228

229   Fig. 6 Static equilibrium condition for the surrounding rock mass.

230
$$\sigma_r r d\omega L_z + 2\sigma_t dr L_z \sin\frac{d\omega}{2} = (\sigma_r + d\sigma_r)(r + dr)d\omega L_z \tag{8}$$

231   Where, σ_r is radial stress, σ_t is tangential stress, r is the radius of the infinitesimal volume, $d\omega$ is the

232   loop angle, dr is the size in the radial direction, L_z is the size in the axial direction.

233   Noticing that $\sin(\frac{d\omega}{2})$ approximately equals $\frac{d\omega}{2}$ since $d\omega$ is an infinitesimal (Alonso1 et

234   al., 2003), the equilibrium equation can be deduced as:

235
$$\frac{d\sigma_r}{dr} = \frac{\sigma_t - \sigma_r}{r} \tag{9}$$

236   When applying Eq. (9) to the elastic region, where the sum of σ_r and σ_t equals $2P_0$, the

equilibrium equation for elastic region can be formulated as:

$$\frac{d\sigma_r}{dr} = \frac{2P_0 - 2\sigma_r}{r} \tag{10}$$

When applying it to the plastic region, where the stress state of rock mass should verify the failure criterion as shown in Eq. (6), the equilibrium equation for the plastic region can be formulated as:

$$\frac{d\sigma_r}{dr} = \frac{(K_p - 1)\sigma_r + \sigma_c}{r} \tag{11}$$

Where, σ_c is a varying parameter which is a function of the major principal plastic strain ε_1^p as shown below:

$$\sigma_c = \begin{cases} \sigma_c(\sigma_3) + \dfrac{(\sigma_c(\sigma_3) - \sigma_c^*(\sigma_3))\varepsilon_1^p}{\alpha\varepsilon_{1e}} & (0 \leq \varepsilon_1^p \leq \alpha\varepsilon_{1e}) \\ \sigma_c^*(\sigma_3) & (\varepsilon_1^p \geq \alpha\varepsilon_{1e}) \end{cases} \tag{12}$$

3.3 Displacement Compatibility Equations for Rock Mass

Due to the plane strain axial symmetry assumption, the strain-displacement relationships for the rock mass can be simplified significantly as:

$$\frac{du}{dr} = \varepsilon_r \quad \frac{u}{r} = \varepsilon_t \tag{13}$$

In the elastic region, according to Hook's law, the tangential strain of the rock mass can be evaluated from its stress state, as formulated in Eq. (14), where E and v are the Young's modulus and the Poisson ratio of the rock mass.

$$\varepsilon_t = (\frac{\sigma_t}{E} - v\frac{\sigma_r}{E} - v\frac{2P_0 v}{E}) - (\frac{P_0}{E} - v\frac{P_0}{E} - v\frac{2P_0 v}{E}) \tag{14}$$

Notice that only the strain caused by tunnel excavation is concerned, which means the initial strain due to in-situ stresses should be removed. Then, associating these two equations and considering the hydrostatic in-situ stress condition, the displacement compatibility equation for the elastic region can be formulated as Eq. (15).

$$u = r\varepsilon_t = \frac{P_0 - \sigma_r}{E}(1 + v)r \tag{15}$$

For the plastic region, the loading path in this problem refers to a monotonic decrease of the fictitious inner pressure, corresponding to the advancing of the tunnel face. Consequently, the rates

261 of all mechanical variables can be evaluated by their first-order derivatives with respect to P_i. The

262 incremental theory of plasticity (Graziani et al., 2005) assumes that the total strain rate consists of

263 both elastic part and plastic part, as shown in Eq. (16). The elastic part is controlled by Hooke's law

264 and the plastic part by the potential flow rule, as formulated by Eqs. (17) and (18), respectively. The

265 relationship between the strain rate and the displacement velocity was simplified by virtue of axial

266 symmetry and formulated by Eq. (19).

267
$$\dot{\varepsilon}_r = \dot{\varepsilon}_r^{\,e} + \dot{\varepsilon}_r^{\,p}, \qquad \dot{\varepsilon}_\theta = \dot{\varepsilon}_\theta^{\,e} + \dot{\varepsilon}_\theta^{\,p} \tag{16}$$

268
$$\dot{\varepsilon}_r^{\,e} = \frac{1-v}{2G}\dot{\sigma}_r - \frac{v}{2G}\dot{\sigma}_\theta, \quad \dot{\varepsilon}_\theta^{\,e} = \frac{1-v}{2G}\dot{\sigma}_\theta - \frac{v}{2G}\dot{\sigma}_r \tag{17}$$

269
$$\dot{\varepsilon}_r^{\,p} = \lambda\frac{\partial g}{\partial\sigma_r} = \lambda, \quad \dot{\varepsilon}_\theta^{\,p} = \lambda\frac{\partial g}{\partial\sigma_\theta} = -\lambda K_\psi \tag{18}$$

270
$$\dot{\varepsilon}_r = \frac{\partial\dot{u}}{\partial r}, \quad \dot{\varepsilon}_\theta = \frac{\dot{u}}{r} \tag{19}$$

271 Here, g is the plastic potential. The rates of all mechanical variables (denoted by a dot mark) are

272 referred as their first-order derivatives with respect to P_i. Then combining these four equations,

273 eliminating the multiplier λ, the displacement compatibility equation for the plastic region can be

274 expressed as:

275
$$\frac{\partial\dot{u}}{\partial r} + K_\psi\frac{\dot{u}}{r} = \frac{(1-v-vK_\psi)}{2G}\dot{\sigma}_r - \frac{(vK_\psi - K_\psi + v)}{2G}\dot{\sigma}_\theta \tag{20}$$

276 **3.4 Semi-analytical Solution**

277   The displacement compatibility equation and the equilibrium equation (together with the

278 failure criterion) can only be solved by numerical methods. The fourth order Runge-Kutta method

279 was employed, and a two dimensional finite difference algorithm (i.e. along the unloading path and

280 along the radial direction) was implemented. All the variables describing the state of the

281 surrounding rock mass have two indices: the first indicates a certain stage in the unloading path and

282 the second indicates a certain position in the radial direction. Supposing that at former stage (say the

283 $(k\text{-}1)^{\text{th}}$ stage where $P_i = P_i^{(k-1)}$), all the mechanical states of the rock mass are known, the objective is

284 to evaluate all the mechanical states at current stage (i.e. the kth stage where $P_i = P_i^{(k)}$) according to

285 their known counterparts at the former stage. The solution includes the following three steps: stress

286 evaluation, displacement evaluation and transitional strength update. After one iteration finished,

287 these known mechanical states at the current stage can be used to evaluate the mechanical states at

288 next stage (i.e. the $(k+1)^{\text{th}}$ stage where $P_i=P_i^{(k+1)}$), following the same three steps. This kind of

289 iteration was repeated until the final stage where $P_i=P_i^{fin}$.

(1) Stress evaluation of rock mass

291 The equilibrium equations (10) and (11) were solved by the fourth-order Runge-Kutta method

292 (Basheer, 2000). At the current stage, the radial stress at the tunnel wall $\sigma_r(k, R_a)$ is known and

293 equals to $P_i^{(k)}$, which serves as the boundary condition of the equilibrium equations. According to

294 Eq. (11) and the failure criterion, the radial and tangential stresses can be obtained by Runge-Kutta

295 method. When the radial stress increases up to the critical inner pressure P_i^{cri}, record the position as

296 the radius of the elasto-plastic interface R_e, then go on evaluating the stress state of elastic region.

297 According to the research of Carranza-Torres (1999), σ_{re} is a constant that only depends on the

298 properties of rock mass itself and independent of the position of the elasto-plastic interface. The

299 critical inner pressure can be calculated by the following formula.

$$P_i^{cri} = \sigma_{re} = \frac{2P_0 - \sigma_c(\sigma_3)}{K_p + 1} \tag{21}$$

301 The radial and tangential stresses at the current stage can be determined after the stress

302 evaluation process.

(2) Displacement evaluation of rock mass

304 For the elastic region, the radial displacement of the rock mass at the current stage can be

305 evaluated directly by the radial stress of rock mass at the current stage, according to Eq. (15). For

306 the plastic region, the radial and tangential stress rates $\dot{\sigma}_r(k,r)$ and $\dot{\sigma}_t(k,r)$ should be first

307 evaluated by their first-order difference with respect to P_i, as shown in Eq. (22).

$$\dot{\sigma}(k,r) = \frac{\sigma(k,r) - \sigma(k-1,r)}{dP_i} \quad (r \leq R_e) \tag{22}$$

309 Similarly, the deformation rate at the elasto-plastic interface $\dot{u}(k,R_e)$, which serves as the

310 boundary condition of the compatibility equation, can also be obtained by its first-order difference

311 with respect to P_i. Then the fourth-order Runge-Kutta method was utilized again to evaluate the

312 deformation rate at each sequential calculation point (inward radial direction) according to the

313 compatibility equations (20). Finally, the displacement at the current stage can be obtained by

314 accumulating the displacement increment at the current stage to its counterpart at the former stage.

315
$$u(k,r) = u(k-1,r) + \dot{u}(k,r)dP_i \quad (r \le R_e) \tag{23}$$

316 The displacement and the stresses at the former stage, as well as the stresses at the current

317 stage, are required during this step. Then the displacement at the current stage can be determined

318 after the displacement evaluation process.

319 (3) Transitional strength update of rock mass

320 After the displacement evaluation, the major principle plastic strain ε_t^p at the current stage,

321 which serves as the softening parameter, can be evaluated by Eq. (24). Then the transitional strength

322 at the current stage can be computed via Eq. (6) and Eq. (7).

323
$$\varepsilon_t^p(k,r) = \varepsilon_t(k,r) - \varepsilon_{te}(k,r) = \frac{u(k,r)}{r} - \frac{u(k,R_e)}{R_e} \quad (r \le R_e) \tag{24}$$

324 The displacements and the tangential stresses at the current stage are required in this step, and

325 the transitional strength of rock mass at the current stage can be determined.

326 After these three steps, all the mechanical states at the current stage are known, which can be

327 used to evaluate their counterparts at next stage (i.e. the $(k+1)^{th}$ stage where $P_i = P_i^{(k+1)}$).

328 **4 Application and Verification of the New Model**

329 The proposed analytical method was programmed in VB development environment, and

330 verified by numerical simulations. An illustrative case study was presented in this section to

331 demonstrate the influence of post-failure behavior in conventional tunnelling. Supposing that a

332 circular tunnel with a design radius of 5.0 m was excavated under a hydrostatic in-situ stress of 10

333 MPa (about 500 m rock mass covering above). The properties of the rock mass employed were

334 listed in Table 3.

335 Fig. 7 showed the ground responses after excavation obtained by the analytical solution

336 (including the distribution of stress, displacement, and transitional strength, represented by solid

337 lines, Analytical_New). To highlight the influence of the different constitutive model, the ground

338 responses with the elastic-perfectly plastic model (Analytical_Ideal) and the conventional

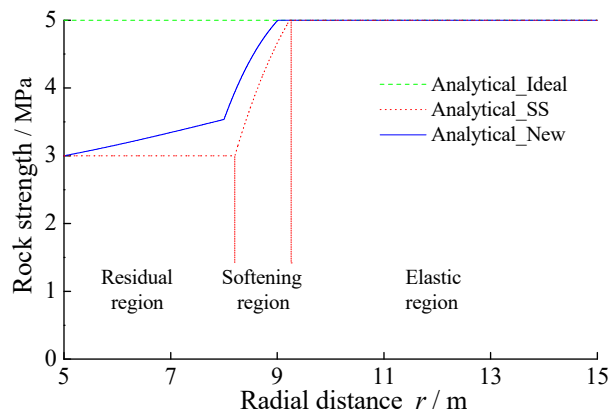339 strain-softening model (Analytical_SS) were also calculated and represented in these figures.

(a)

(b)

(c)
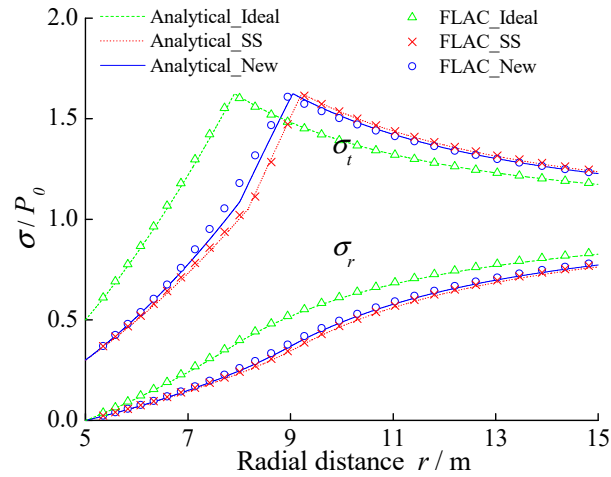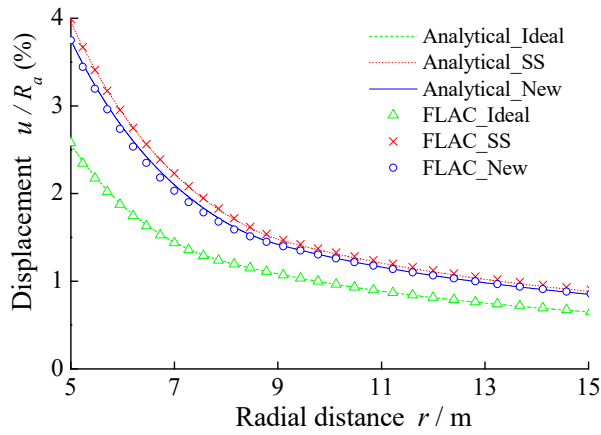
Fig. 7 Ground responses of a circular tunnel: (a) stress distributions; (b) displacement distributions; (c) transitional strength distributions.

The analytical results showed that the plastic region and the displacement from the new model fall between the elastic-perfectly plastic and the conventional strain-softening solution. For the new model, the plastic region and the displacement is smaller than the conventional strain-softening

351   model due to the increasing of post-peak strength. In this calculation case, the difference in the

352   maximum displacements is about 5%. Although the value is not very large compared with the actual

353   error between the theoretical results and measured data, eliminating the system errors is a

354   meaningful work. The influence rules of various parameters on the deformation and failure of rock

355   mass will be revealed in the following parameters analysis.

356   As shown in Fig. 7c, the equivalent transitional strength in the elastic region is constant, and

357   no softening appears. The equivalent transitional strength distributions in the surrounding rock mass

358   is influenced by the confining pressure and the principal plastic strain in the plastic region. The

359   plastic region is divided into residual region and softening region according to the principal plastic

360   strain. In the residual region, the equivalent transitional strength is constant in the conventional

361   strain-softening model. While, the equivalent transitional strength increases with the increasing of

362   confining pressure (σ_r) in the modified strain-softening model.

363   The validity of analytical method was verified by numerical simulations (codes: FLAC^{3D}). The

364   new model in the numerical simulations was developed based on the strain-softening model by the

365   Fish language in FLAC^{3D}. The transitional strength was updated according to the stress and

366   deformation state of every element after every step. The results from the numerical simulations

367   were represented in Fig. 7 (denoted by triangle, cross and circle marks for three different models

368   respectively). As shown in these figures, the ground responses computed by the analytical method

369   and by the numerical simulations fit each other almost exactly.

370   **5 Parameters Analysis**

371   Parameters analysis was performed to study the influence of different parameters in the new

372   model quantitatively. The studied parameters included the equivalent peak strength $\sigma_c(0)$, the

373   equivalent residual strength $\sigma_c^*(0)$ and the exponential factor γ. Taking the illustrative case above as

374   a standard one and varying a single parameter, the relative influence of different parameters on the

375   deformation and failure characteristics of rock mass was illustrated.

376   The tunnel convergence was selected as the estimation index. The error between the results of

377   strain-softening model and the new model was defined as Eq. (25), which physically stranded for

378   the ratios of tunnel convergence.

$$err_{\max} = \frac{u_{SS} - u_{New}}{u_{SS}} \qquad (25)$$

Where, u_{ss} is the maximum tunnel convergence with strain-softening model, u_{New} is the maximum tunnel convergence with the new model.

5.1 The Influence of Equivalent Peak Strength

The equivalent peak strength of rock mass was selected to study its influence on the tunnel convergence. As the equivalent residual strength was 3 MPa in the standard case, the equivalent peak strength was set from 3 MPa to 17 MPa in the following examples. Meanwhile, the other parameters were the same with the standard case.
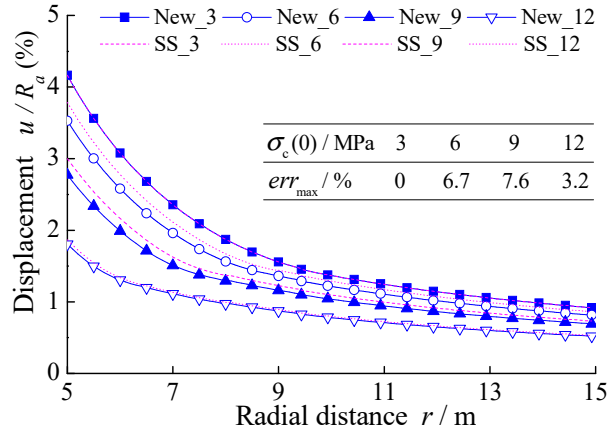
The evolution of the maximum displacement with the increasing of equivalent peak strength is shown in Fig. 8a. To highlight the difference, the result of the strain-softening model and the $err_{\max}$ were also calculated and depicted in this figure. In the strain-softening model, the peak strength σ_c^1 and the residual strength σ_c^2 are considered to be equal to the equivalent peak strength $\sigma_c(0)$ and the equivalent residual strength $\sigma_c^*(0)$, respectively.
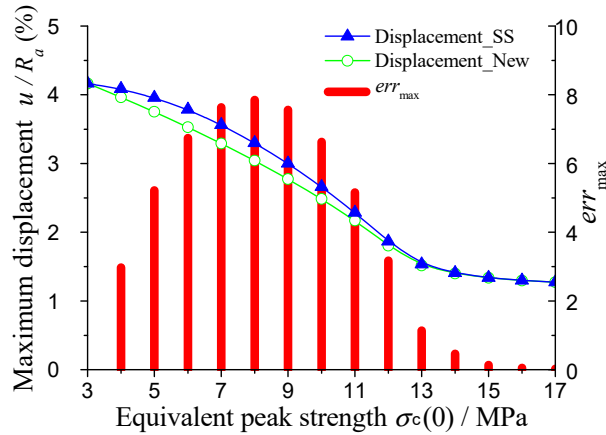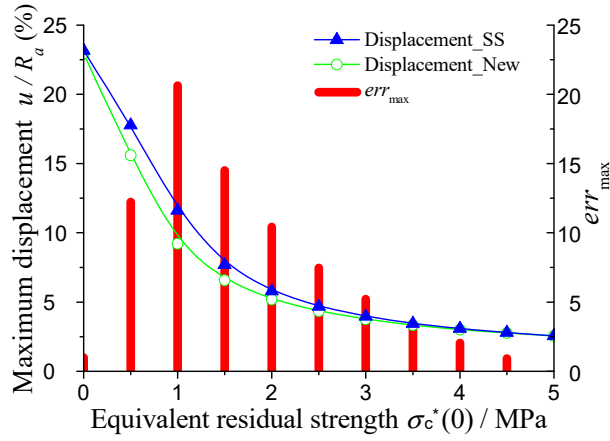

(a)

Fig. 8 The influence of equivalent peak strength: (a) evolution of the maximum displacement and the error; (b) displacement distribution of some typical cases.

The results showed that the maximum displacement in both models decreased gradually with the increasing of equivalent peak strength. The err_{max} increased first and then decreased, and reach the maximum value for $\sigma_c(0) = 8$ MPa. When the equivalent peak strength is very low, the difference between the equivalent peak strength and the equivalent residual strength is very small, which certainly resulting in a small err_{max} value. When the equivalent peak strength is very high, the plastic zone is very small. Therefore, the influence of post peak behaviors decreased, which resulting in a small err_{max} value. The displacement distribution of some typical cases in the surrounding rock mass are shown in Fig. 8b. This figure showed that the displacement difference between the two models mainly located in the plastic zone.

5.2 The Influence of Equivalent Residual Strength

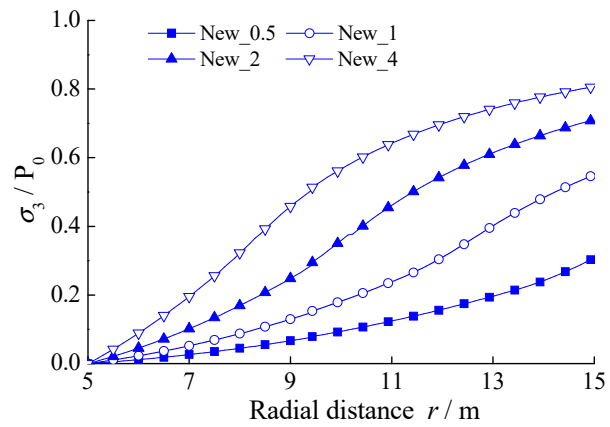The influence of equivalent peak strength was studied in this part. As the equivalent peak strength is 5 MPa in the standard case, the equivalent residual strength was set from 0MPa to 5MPa in the following examples. The other parameters were also same with the standard case. The evolutions of the maximum displacement and the err_{max} with the increasing of equivalent residual strength are shown in Fig. 9a.

413

414

(a)

415

416

(b)

$\sigma_c^{\star}(0)$ / MPa	0.5	1	2	4
err_{max} / %	12.2	20.6	10.4	2.0
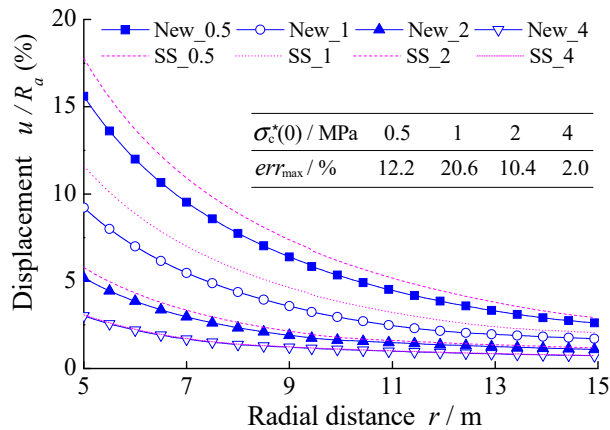
417

418

(c)

419   Fig. 9 The influence of equivalent residual strength: (a) evolution of the maximum displacement

420   and the error; (b) distributions of confining pressure; (c) displacement distributions of some typical

421   cases.

422   The results showed that the maximum displacement decreased sharply with the increasing of

423   equivalent residual strength. The err_{max} increased first and then decreases, and reached the

424 maximum value at the stage of 1 MPa. When the equivalent residual strength was close to the

425 equivalent peak strength (5MPa), the small difference also resulted in small err_{max} value. However,

426 when the equivalent residual strength was small (between 0MPa and 1MPa), meanwhile the

427 difference was very large, the err_{max} also became smaller. This behaviour depends on the small

428 value of confining pressure in case of small equivalent residual strength as shown in Fig. 9b. The

429 displacement distributions of some typical cases in the surrounding rock mass are shown in Fig. 9c.

430 **5.3 The Influence of Exponential Factor**

431   The influence of exponential factor was studied in this part. It was set from 0.01 to 10 in the

432 following examples. The other parameters were also the same with the standard case. The

433 evolutions of the maximum displacement and the err_{max} with the increasing of equivalent residual
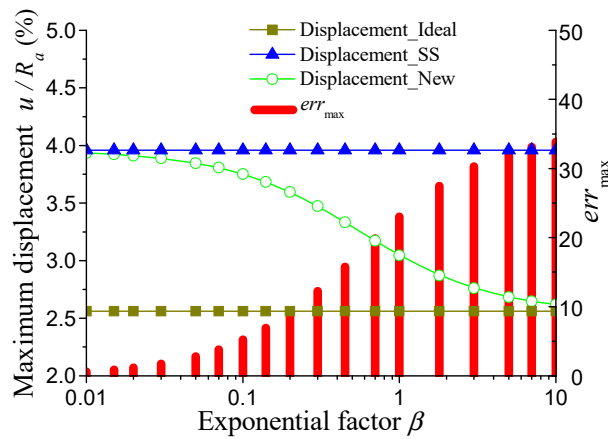
434 strength are shown in Fig. 10a. The results of elastic-perfectly plastic model and strain-softening

435 model are also shown in this figure.

436

437   (a)

438

439   (b)

(c)
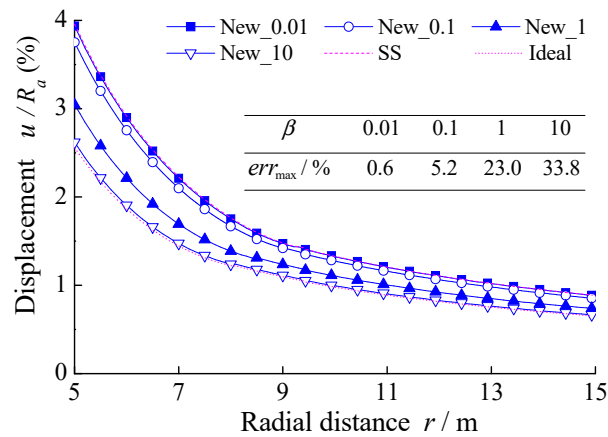
442   Fig. 10 The influence of exponential factor: (a) evolution of the maximum displacement and the

443   error; (b) displacement distribution of some typical cases; (c) distributions of equivalent residual

444   strength for different value of exponential factors.

445   The results showed that the maximum displacement from the new model decreased gradually
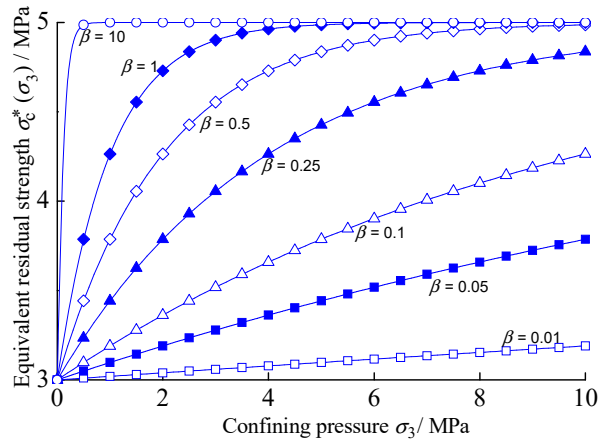
446   with the increasing of exponential factor. The error between the results of strain-softening model

447   and the new model err_{max} increased monotonously. There was a clearly trend that the maximum

448   displacement from the new model gradually approaching the elastic-perfectly plastic model from

449   the strain-softening model with the increasing of exponential factor. This behaviour can also be seen

450   in Fig. 10b. It can be explained by the distribution of equivalent residual strength with different

451   value of exponential factor as shown in Fig. 10c. The essential difference of the new model and the

452   elastic-perfectly plastic model, the strain-softening model was herein revealed.

453   The results above showed that the post-peak behaviour of rock mass influenced the tunnel

454   convergence dramatically. According to parameter studies, the error between the results of

455   strain-softening model and the new model was estimated to range from 0% to 35% in common

456   conditions.

457   **6 Conclusions**

458   A modified strain-softening model was proposed to describe the non-linear evolution of

459   residual strength of rock mass under the influence of confining pressure. The new model can

460   simulate the gradually transition from strain-softening features to elastic-perfectly plastic with the

461   increasing of confining pressure.

462   In the new model, equivalent residual strength was defined to describe the actual behaviour of

463 rocks. Based on the laboratory test data, the relation between the equivalent residual strength and

464 confining pressure was represented by a negative exponential function. The parameters were

465 estimated by curvilinear regression based on a series of stress-strain curves under common triaxial

466 compression. The values of correlation coefficient were greater than 0.7 for all the rock samples,

467 which indicated that the correlation between equivalent residual strength and confining pressure

468 was very significant.

469   Based on the plane strain axial symmetry assumption and the incremental theory of plasticity,

470 equilibrium equations and compatibility equations of rock mass around a circular tunnel were

471 deduced theoretically. The equations were programmed in the Visual Basic development

472 environment, and a semi-analytical solution was achieved. The influence of post-failure behavior of

473 rocks was demonstrated through an illustrative case study. The distribution of stress, displacement,

474 and transitional strength around the circular tunnel were presented. The differences between the

475 elastic-perfectly plastic model, the strain-softening model and the new model was estimated

476 quantitatively. In addition, the validity of proposed method was verified by numerical simulations.

477   Parameters analysis showed that the post-peak behaviour of rock mass influenced the tunnel

478 convergence dramatically. According to parameter studies, the error between the results of

479 strain-softening model and the new model was estimated to range from 0% to 35% in common

480 conditions.

481

Reference

Alonso, E., Alejano, L.R., Varas, F., Fdez-Manin G., Carranza-Torres C., 2003. Ground response curves for rock masses exhibiting strain-softening behaviour. Int. J. Numer. Anal. Meth. Geomech. 27, 1153–1185.

Alejano, L.R., Rodriguez, D.A., Alonso, E., Fdez-Manin, G., 2009. Ground reaction curves for tunnels excavated in different quality rock masses showing several types of post-failure behaviour. Tunn. Undergr. Sp. Technol. 24, 689–705.

Alejano, L.R., Alonso, E., Rodriguez, D.A., Fernandez, M.G., 2010. Application of the convergence-confinement method to tunnels in rock masses exhibiting Hoek-Brown strain-softening behaviour. Int. J. Rock Mech. Min. Sci. 47, 150–160.

Basheer, I., Hajmeer, M., 2000. Artificial neural network: fundamentals, computing, design and application. J. Microbiol. Meth. 43(1), 3–31.

Besuellea, P., Desruesb, J., Raynaud, S., 2000. Experimental characterisation of the localisation phenomenon inside a Vosges sandstone in a triaxial cell. Int. J. Rock Mech. Min. Sci. 37, 1223–1237.

Carranza-Torres C., Fairhurst, C., 1999. The elasto-plastic response of underground excavations in rock masses that satisfy the Hoek-Brown failure criterion. Int. J. Rock Mech. Min. Sci. 36(6), 777–809.

Cheng, C., Chen, X., Zhang, S., 2016. Multi-peak deformation behavior of jointed rock mass under uniaxial compression: Insight from particle flow modeling. Eng. Geol. 213(4), 25–45.

Cui, L., Zheng, J.J., Dong, Y.K., Zhang, B., Wang, A., 2017. Prediction of critical strains and critical support pressures for circular tunnel excavated in strain-softening rock mass. Eng. Geol. 224, 43–61.

Fang, Z., Harrison, J.P., 2001. A mechanical reduction index for rock. Int. J. Rock. Mech. Min. Sci. 38(8), 1193–1199.

Graziani, A., Boldini, D., Ribacchi, R., 2005. Practical estimate of deformations and stress relief factors for deep tunnels supported by shotcrete. Rock Mech. Rock Eng. 38(5), 345–372.

Guan, Z.C., Jiang, Y.J., Tanabasi, Y., 2007a. Reinforcement mechanics of passive bolts in conventional tunnelling. Int. J. Rock Mech. Min. Sci. 44(4), 625–636.

Guan, Z.C., Jiang, Y.J., Tanabasi, Y., 2007b. Ground reaction analyses in conventional tunneling

515   excavation. Tunn. Undergr. Sp. Technol. 22(2), 230–237.

516   Hao, X.J., Feng, X.T., Yang, C.X., Jiang, Q., Li, S.J., 2016. Analysis of EDZ development of

517   columnar jointed rock mass in the Baihetan diversion tunnel. Rock Mech. Rock Eng. 49,

518   1289–1312.

519   Indraratna, B., Nimbalkar, S., Coop, M., Sloan, S.W., 2014. A constitutive model for coal-fouled

520   ballast capturing the effects of particle degradation. Comput. Geotech. 61, 96–107.

521   Jiang, Y., Yoneda, H., Tanabashi, Y., 2001. Theoretical estimation of loosening pressure on tunnels

522   in soft rocks. Tunn. Undergr. Sp. Technol. 16(2), 99–105.

523   Juang, C.H., Luo, Z., Atamturktur, S., Huang, H., 2013. Bayesian Updating of Soil Parameters for

524   Braced Excavations Using Field Observations. J. Geotech. Geoenviron. 139(3), 395–406.

525   Kaiser, P.K., Kim, B.H., 2015. Characterization of Strength of Intact Brittle Rock Considering

526   Confinement-Dependent Failure Processes. Rock Mech. Rock Eng. 48, 107–119.

527   Li, W., Li, S., Feng, X., 2011. Study of post-peak strain softening mechanical properties of rock

528   based on Mohr-Coulomb criterion. Chin. J. Rock. Mech. Eng. 30(7), 1460–1466.

529   Li, X., Cao, W., Su, Y., 2012. A statistical damage constitutive model for softening behavior of

530   rocks, Eng. Geol. 143-144, 1–17.

531   Liu, Q., Liu, K., Zhu, J., Lu, X., 2014. Study of mechanical properties of raw coal under high stress

532   with triaxial compression. Chin. J. Rock Mech. Eng. 33(1), 24–34.

533   Lu, Y., Wang, L., Yang, F., 2010. Post-peak strain softening mechanical properties of weak rock.

534   Chin. J. Rock Mech. Eng. 29(3), 640–648.

535   Ma, L., Xu, H., Tong, Q., Dong, L., Zhang, N., Li, J., 2014. Post-yield plastic frictional parameters

536   of a rock salt using the concept of mobilized strength. Eng. Geol. 177, 25–31.

537   Peng, J., Cai, M., Rong, G., Yao, M.D., Jiang, Q.H., Zhou, C.B., 2017. Determination of

538   confinement and plastic strain dependent post-peak strength of intact rocks. Eng. Geol. 218,

539   187–196.

540   Saksala, T., Ibrahimbegovic, A., 2014. Anisotropic viscodamage-viscoplastic consistency

541   constitutive model with a parabolic cap for rocks with brittle and ductile behaviour. Int. J.

542   Rock Mech. Min. Sci. 70, 460–473.

543   Shen, H., Wang, S., Liu, Q., 2014. Simulation of constitutive curves for strain-softening rock in

544   triaxial compression. Rock Soil Mech. 35(6), 1647–1654.

545   Tiwari, R.P., Rao, K.S., 2006. Post failure behaviour of a rock mass under the influence of triaxial

546   and true triaxial confinement. Eng. Geol. 84, 112–129.

Troncone, A., Conte, E., Donato, A., 2014. Two and three-dimensional numerical analysis of the progressive failure that occurred in an excavation-induced landslide. Eng. Geol. 183, 265–275.

Tutluoğlu, L., Öge, İ.F., Karpuz, C., 2015. Relationship between pre-failure and post-failure mechanical properties of rock material of different origin. Rock Mech. Rock Eng. 48, 121–141.

Varas, F., Alonso, E., Alejano, L., Fdez-Manin, G., 2005. Study of bifurcation in problem of unloading a circular excavation in a strain-softening material. Tunn. Undergr. Sp. Technol. 20(4), 311–322.

Walton, G., Arzua, J., Alejano, L.R., Diederichs, M.S., 2015. A laboratory-testing-based study on the strength, deformability, and dilatancy of carbonate rocks at low confinement. Rock Mech. Rock Eng. 48(3), 941–958.

Wang, J.A., Park, H.D., 2002. Fluid permeability of sedimentary rocks in a complete stress–strain process. Eng. Geol. 63, 291–300.

Wu X., Jiang Y., Li B., 2018a Influence of joint roughness on the shear behaviour of fully encapsulated rock bolt. Rock Mech. Rock Eng. 51(3): 953–959.

Wu X., Jiang Y., Guan Z., Wang G., 2018b. Estimating the support effect of the energy-absorbing rock bolt based on the mechanical work transfer ability, Int. J. Rock Mech. Min. Sci. 103: 168-178.

Yang, S.Q., Jiang, Y.Z., Xu, W.Y., Chen, X.Q., 2008. Experimental investigation on strength and failure behavior of pre-cracked marble under conventional triaxial compression. Int. J. Solids Struct. 45, 4796–4819.

You, M., Su, C., Gou, Y., 2007. Experimental study on strength and deformation properties of hollow cylindrical specimens of marbles. Chin. J. Rock Mech. Eng. 26(12), 2420–2429.

Zhou, H., Yang, F., Zhang, C., Xu, R., Zhang, K., 2012. An elastoplastic coupling mechanical model for marble considering confining pressure effect. Chin. J. Rock Mech. Eng. 31(12), 2389–2399.

Zimbardo, M., 2016. Mechanical behaviour of Palermo and Marsala calcarenites (Sicily), Italy. Eng. Geol. 210(5), 57–69.

Zhang, Q., Zhang C., Jiang B., Li N., Wang Y., (2018) Elastoplastic coupling solution of circular openings in strain-softening rock mass considering pressure-dependent effect. International Journal of Geomechanics, 18(1), 04017132

Appendix A. Strength parameters for different kinds of rocks

The strength parameters for different kinds of marble, mudstone, limestone, coal and sandstone were presented in Tables A1-A9.

Table A.1 Estimation of the equivalent residual strength of Marble T2b (data from Zhou et al. (2012))

Confining pressure	Peak strength	Residual strength	Equivalent peak strength	Equivalent residual strength
0	162	50	160.25	50.00
5	170	70	160.25	57.55
10	186	92	160.25	67.10
20	210	135	160.25	85.20
40	260	225	160.25	125.40

Table A.2 Estimation of the equivalent residual strength of Fine crystal marble (data from You et al. (2007))

Confining pressure	Peak strength	Residual strength	Equivalent peak strength	Equivalent residual strength
0	48	2	55	2.00
5	73	28	55	14.40
10	86	64	55	36.80
20	110	100	55	45.60
40	162	162	55	53.20

Table A.3 Estimation of the equivalent residual strength of Medium crystal marble (data from You et al. (2007))

Confining pressure	Peak strength	Residual strength	Equivalent peak strength	Equivalent residual strength
0	65	2	65.12	2.00
5	81	38	65.12	22.37
10	95	72	65.12	40.74
20	128	115	65.12	52.47
30	162	156	65.12	62.21
40	188	186	65.12	60.95

Table A.4 Estimation of the equivalent residual strength of Coarse marble (data from Yang et al. (2008))

Confining pressure	Peak strength	Residual strength	Equivalent peak strength	Equivalent residual strength
0	68	4	74	4.00
5	90	45	74	31.00

10	108	77	74	49.00
20	131	116	74	60.00
30	155	144	74	60.00

590

591 Table A.5 Estimation of the equivalent residual strength of Marble (data from Shen et al. (2014))

Confining pressure	Peak strength	Residual strength	Equivalent peak strength	Equivalent residual strength
10	102.4	65.3	85.17	41.64
20	135.8	109.5	85.17	62.18
40	188	165.7	85.17	71.07
60	224.5	216.6	85.17	74.65
70	248.3	246.3	85.17	80.69

592

593 Table A.6 Estimation of the equivalent residual strength of Shanxi mudstone (data from Lu et al. (2010))

Confining pressure	Peak strength	Residual strength	Equivalent peak strength	Equivalent residual strength
0	21.1	8.9	24.45	8.90
5	31.4	18.2	24.45	12.78
10	38.1	25.7	24.45	14.86
20	47.1	35	24.45	13.32
30	54.6	48.2	24.45	15.68
40	66.5	66.5	24.45	23.14

594

595 Table A.7 Estimation of the equivalent residual strength of Indiana limestone (data from Walton et al. (2015))

Confining pressure	Peak strength	Residual strength	Equivalent peak strength	Equivalent residual strength
1	67	18	63.71	14.32
2	71	22	63.71	14.65
4	78	33	63.71	18.30
6	87	60	63.71	37.95
8	93	66	63.71	36.60
10	101	75	63.71	38.24
12	107	83	63.71	38.89

596

597 Table A.8 Estimation of the equivalent residual strength of Vosges sandstone (data from Besuellea et al.

598 (2000))

Confining pressure	Peak strength	Residual strength	Equivalent peak strength	Equivalent residual strength
10	83	65	67.7	44.30

20	113	93	67.7	51.60
30	135	114	67.7	51.90
40	150	136	67.7	53.20
50	168	158	67.7	54.50

599

600   Table A.9 Estimation of the equivalent residual strength of typical coal samples (data from Liu et al. (2014))

Confining pressure	Peak strength	Residual strength	Equivalent peak strength	Equivalent residual strength
0	23	1	30.71	1.00
10	62	32	30.71	5.69
20	87	63	30.71	10.37
30	114	95	30.71	16.06
40	135	116	30.71	10.74
50	158	146	30.71	14.43

601

602

Appendix B. Implementation of the new constitutive model by numerical tests

In order to verify the new constitutive model, some numerical simulations were conducted to reproduce the post-failure behavior of the rocks by FLAC^{3D} code. The new model in the numerical simulations was developed based on the strain-softening model by the Fish language in FLAC^{3D}. The transitional strength was updated according to the stress and deformation state of every element after every step. The modified strain-softening constitutive laws in FLAC^{3D} were characterized by six parameters: bulk modulus K, shear modulus G, friction angle ϕ, cohesion c, dilation angle ψ, softening parameter η and the two new parameters β and γ.

The performance of the present model was demonstrated at the material point level using a computational model of a single 8-node cube element. The model size is 1m×1m×1m. The material properties of Tennessee marble and model parameters given in Table B1 were used throughout simulations. The confining pressures were set to be 0MPa, 27.6MPa, 34.5MPa, 48.3MPa in different tests. Compressive axial loading was applied in the form of a velocity boundary condition with a constant velocity of -5×10^{-7} m/s on the upper surfaces.

The numerical test results at different confining pressure are shown in Fig. B.1. To highlight the advantages of the new model, the stress-strain curves with the conventional strain-softening model and results from the laboratory experiments are also depicted in these figures. A better agreement was observed between numerical results with the new model and the experiment data in these figures.
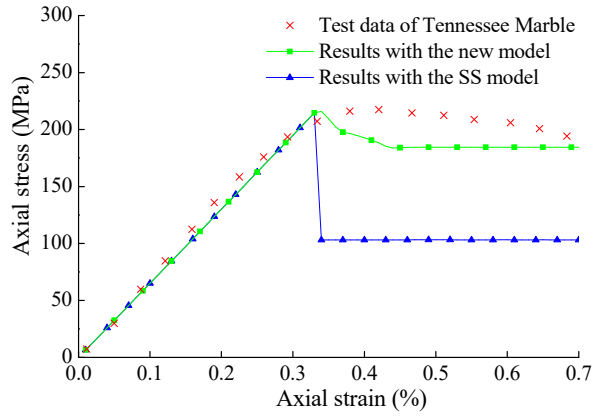
At the condition of σ_3=0 MPa, the rock behaviour with different model are all the same, and close to the experiment data. It is reasonable as no confining pressure is applied, resulting no effect on the residual strength. With the increasing of confining pressure, the advantages of the new model becomes more and more obvious.
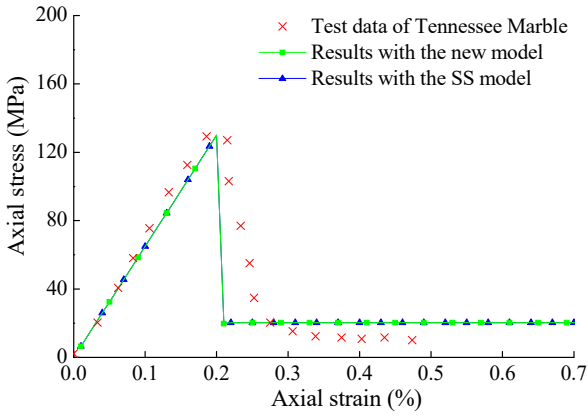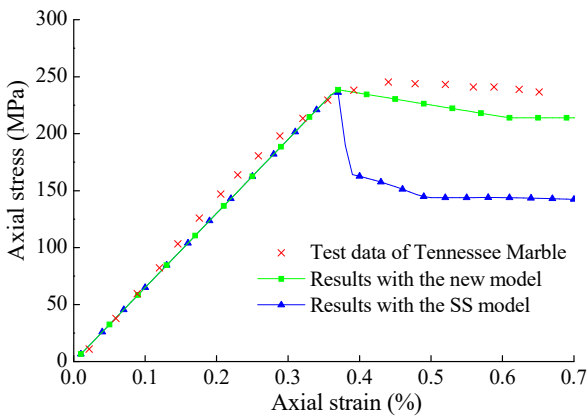
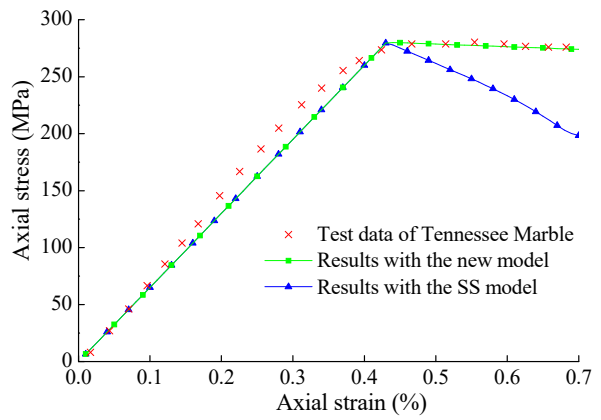Fig. B.1 Comparison between experimental and theoretical curves at different confining pressures: (a) σ_3=0 MPa; (b) σ_3=27.6 MPa; (c) σ_3=34.5 MPa; (d) σ_3=48.3 MPa.

Table B.1 The properties of Tennessee marble employed in the verification case

E/GPa	v	K_p	K_ψ	$\sigma_c(0)$/MPa	$\sigma_c^*(0)$ /MPa	α	β	γ
65	0.2	3.0	1.33	138	20.3	0.005	1.15e8	0.0044